Electronic Supplementary Material (ESI) for RSC Advances.

Supporting Information

Strategy to Synthesise Nano-engineered Polymer Nanocomposite with Mechanically Strong Interface: A Highly Flexible Ammonia Gas Sensor

Payal Mazumdar[1] Sreekumar Chockalingam[2] and Sunita Rattan[1a]*

[1]Amity Institute of Applied Sciences, Amity University Uttar Pradesh,
Sector-125, Noida, India

[2]Physics of Energy Harvesting Division, National Physical Laboratory,
New Delhi-110021, India

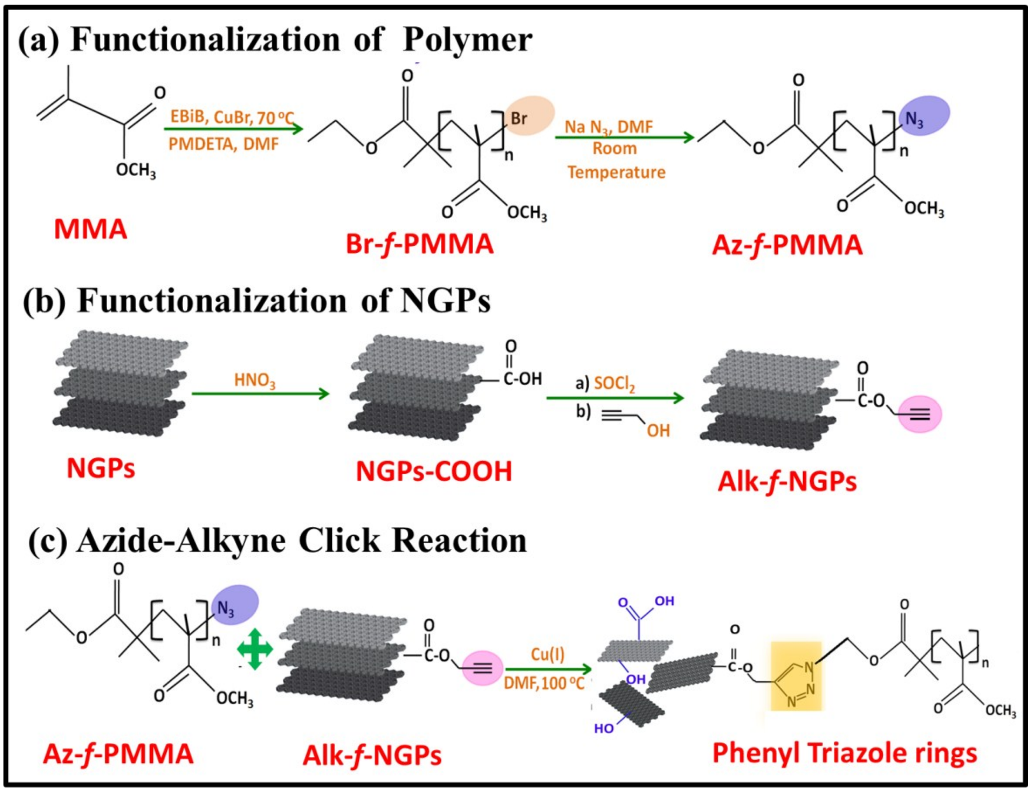

Figure. S1 Synthetic routes for the **(a)** preparation of well-defined azide functionalized PMMA, via ATRP reaction, **(b)** preparation of alkyne-functionalized NGPs, via reaction with thionyl chloride and propargyl alcohol, and **(c)** preparation of polymer nanocomposites via azide-alkyne click coupling.

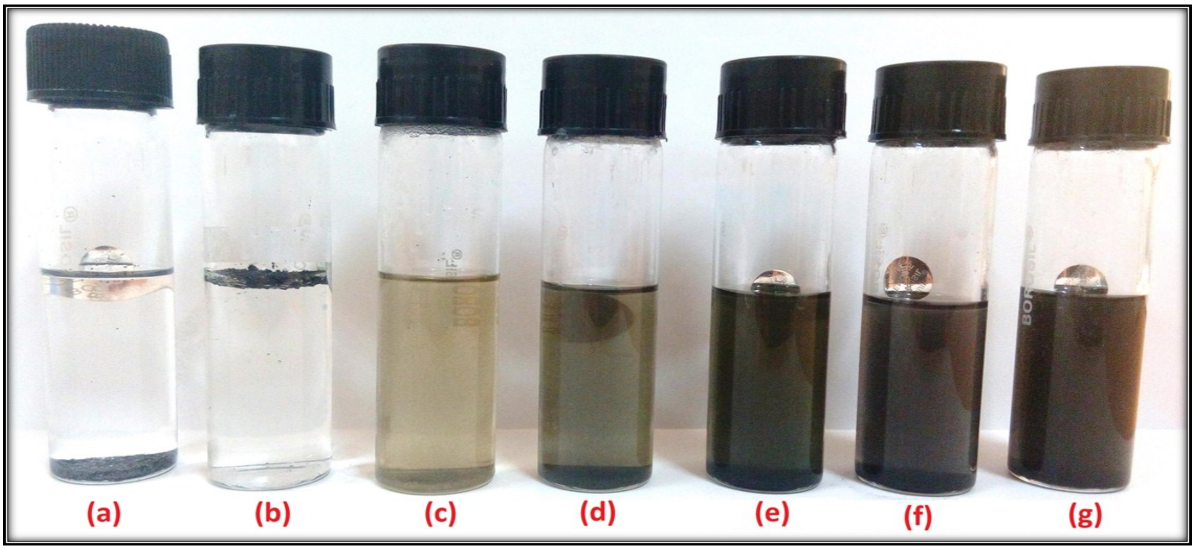

Figure. S2 Digital photographs for the dispersion status in THF of **(a)** Pristine NGPs **(b)** Alk-f-NGPs **(c)** P-NC0.1 **(d)** P-NC0.2 **(e)** P-NC0.3 **(f)** P-NC0.4 **(g)** P-NC0.5.

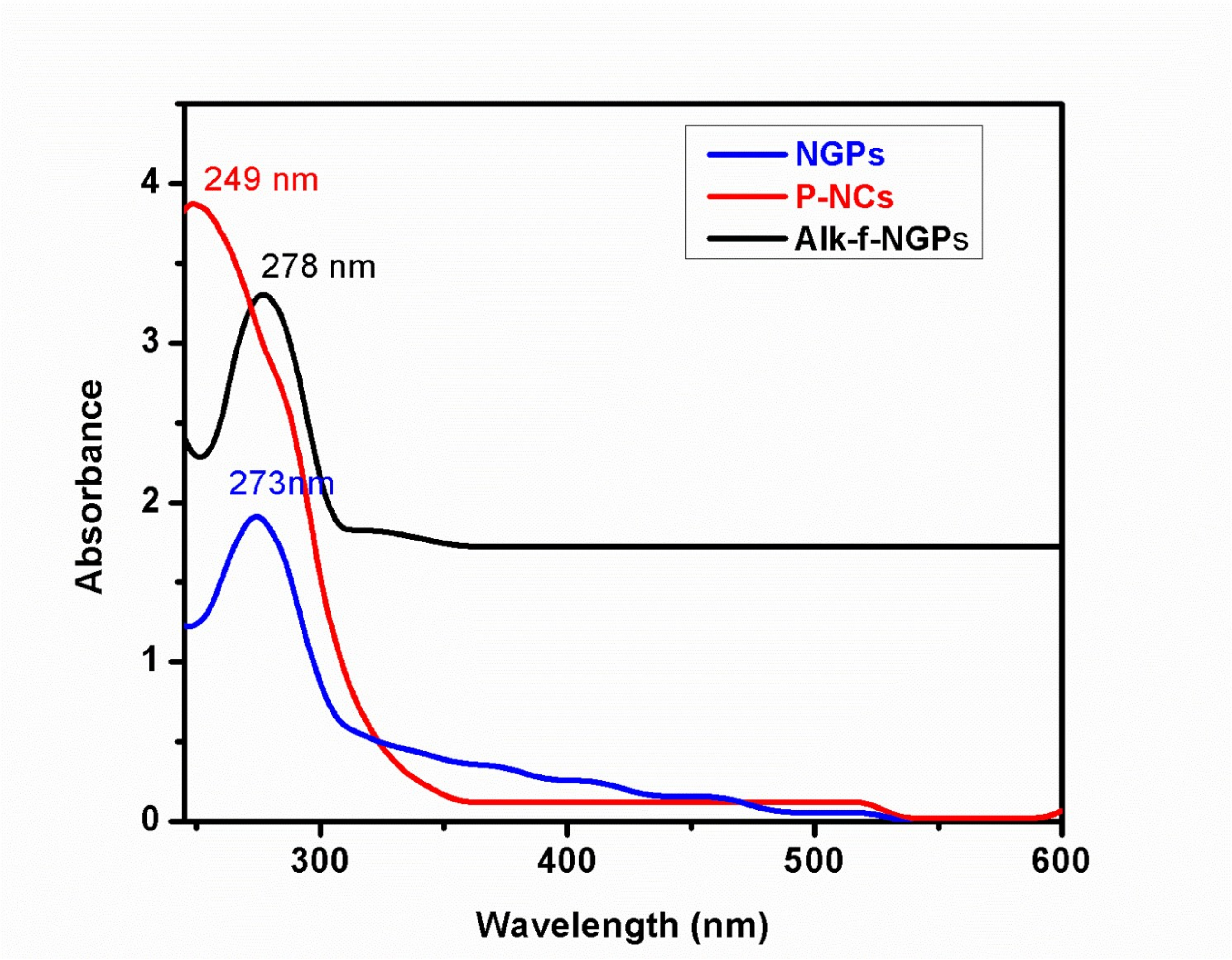

Figure S3. UV-vis absorption spectra of (**a**) NGPs **(b)** Alk-f-NGPs and **(c)** P-NCs.

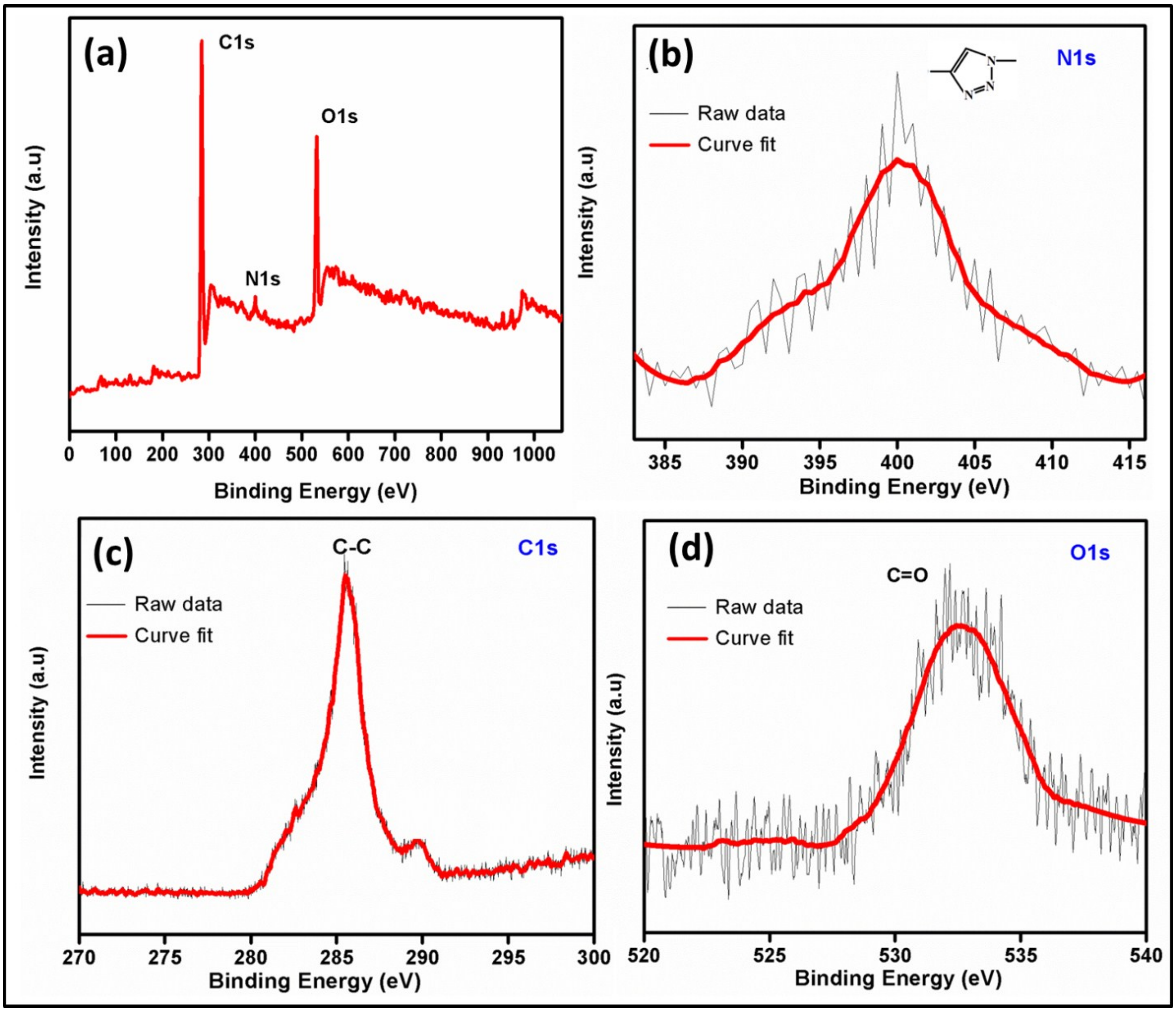

Figure S4. (a) Wide-scan X-ray photoelectron spectra of P-NCs. **(b)** High-resolution N1s spectra (**c**) C1s spectra and **(d)** O1s spectra of P-NCs.

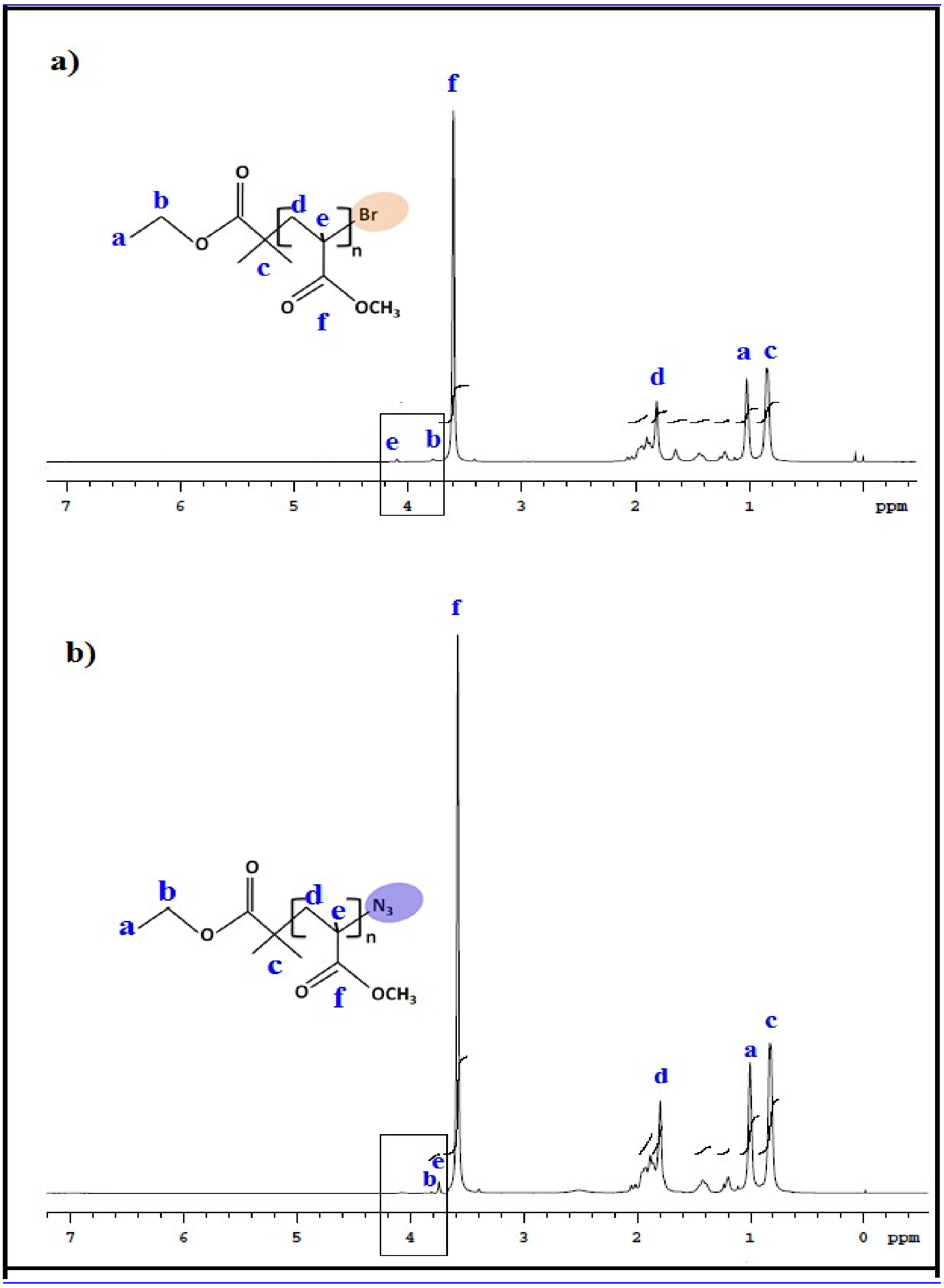

Figure. S5.(a) ^{1}H NMR spectra of bromine-functionalized PMMA obtained by ATRP technique**. (b)** ^{1}H NMR spectra of azide-functionalized PMMA. The spectra were recorded at room temperature in $CDCl_3$.

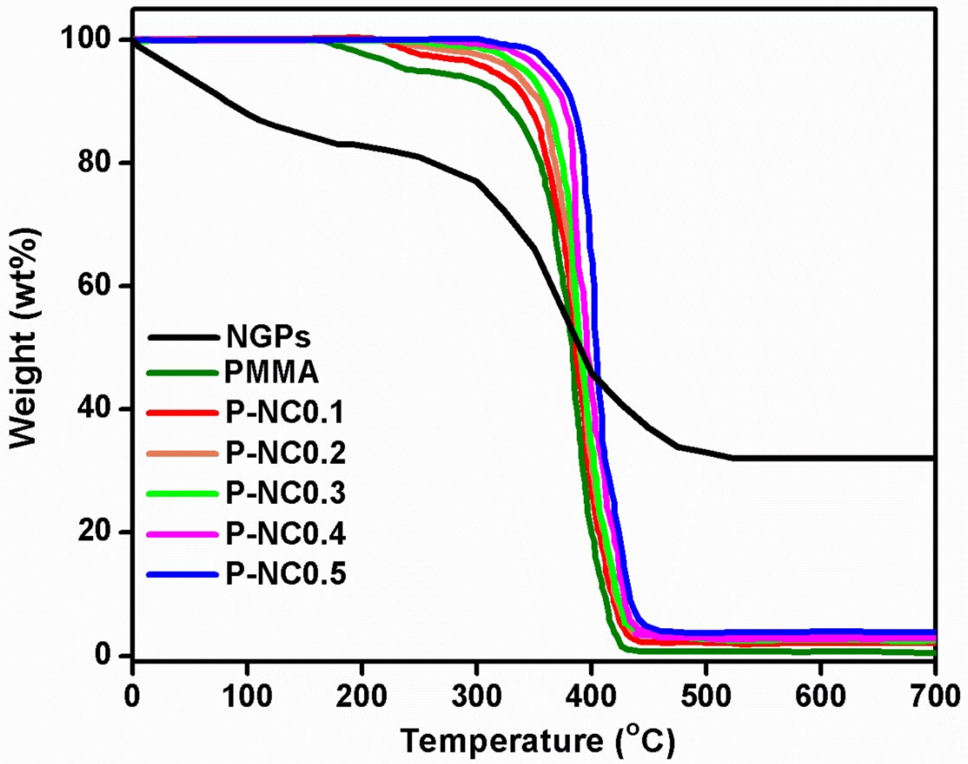

Figure. S6 TGA curves of NGPs, pure PMMA, P-NCs at various NGP loadings.

1. Nanoindentation Measurement of Polymer Nanocomposites

The nanoindentation measurements were carried out on the P-NC films with different loadings of NGPs in order to study their mechanical properties. P-NCs were attached with a specimen mounting wax and crystal bond on a metallic specimen holder with a magnetic base. Extreme care was taken to maintain parallelism while mounting the specimen to the sample holder. Thermal drift occurs when the indenter and the specimen change dimension(s) during a test, as a result of the temperature change. This change in dimension will be registered by the displacement sensor and interpreted as a change in penetration depth, thus leading to a source of error in the results. For best results, the entire system is left for four hours to attain thermal equilibrium, before testing begins to eliminate the error due to thermal drift. It is very important to use accurate dimensions of the indenter for the analysis of the results. For the Berkovich indenter, the radius of the tip can vary depending on the quality of the manufacture. To account for these variations in indenter geometry, an area function is applied to the result, which is a ratio expressed as a function of the plastic depth. For best results, a series of indentations were made on the sample and the average values used for the calculation.

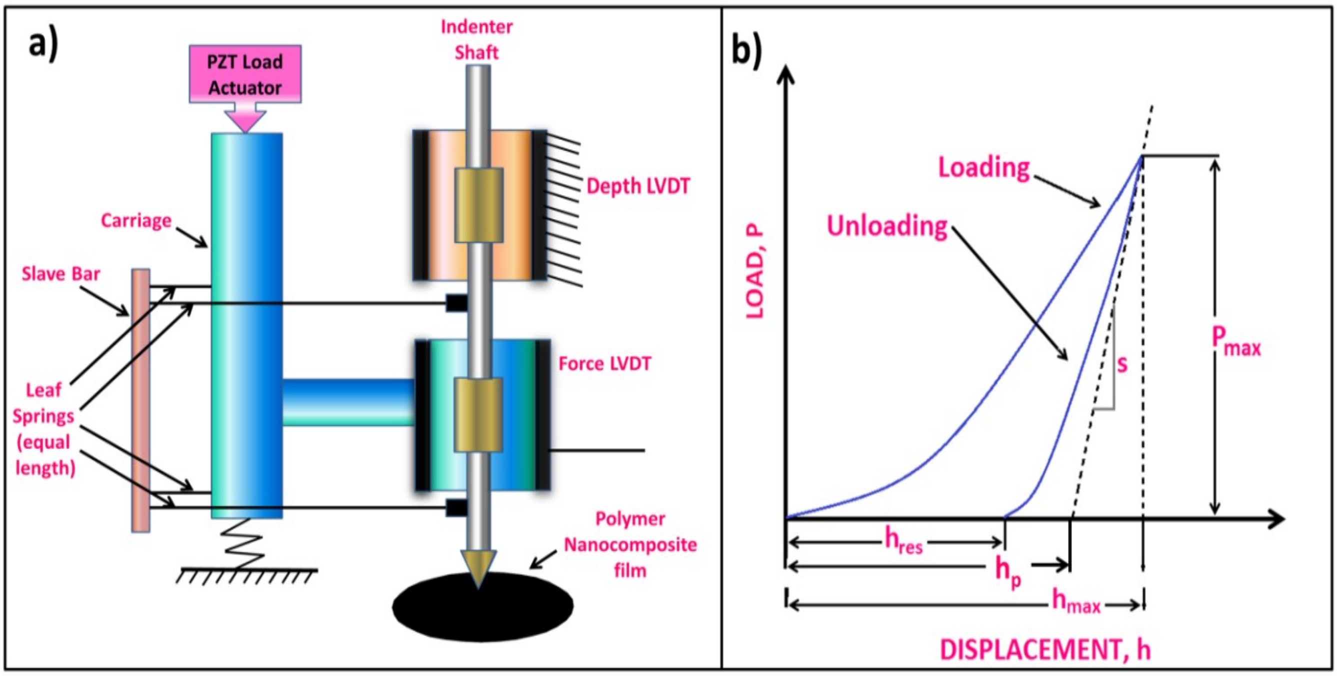

Figure. S7 The schematic of **(a)** the operating principle of the IBIS nanoindentation system, and **(b)** loading and unloading curves from a nanoindentation test.

Figure. S7 shows a schematic of the operation principle of the IBIS nanoindentation system. The IBIS is a load-controlled nanoindentation instrument. A particular feature of this instrument is that the parallel spring load feedback system ensures that the load applied is equal to the set load. It is well accepted that environmental conditions, such as thermal drift and electrical interference, have a deleterious effect on nanoindentation test results. The thermal and the electrical interference due to the surrounding environment are isolated by enclosing the instrument in a plastic enclosure with glass wool insulation. The IBIS nanoindenter applies a very low load, of the order of milli Newtons, with the help of a piezoelectric element, connected to the indentor shaft by leaf springs. The deflection, along with the displacement of the indenter shaft relative to the loading frame, is measured by using linear variable differential transformers (LVDTs). The software used to control the IBIS nanoindenter uses a partial unloading technique to determine the contact stiffness at each load increment of the sample as a function of penetration depth. The software automatically corrects for thermal drift, calculates the initial penetration depth and calibrates the indenter area function. We confirmed the repeatability by performing a series of indentations at 1 mN at different locations of the fused silica reference sample. Figure Sb shows a typical loading-unloading curve obtained by the nanoindentation test. The parameter, h_{res}, is the depth of residual impression, h_{max} is the maximum penetration depth of the indentor, hp is the depth of the residual impression for an equivalent punch, Pmax is the maximum load, and S is the slope of elastic unloading (S = dp/dh). The shape of the load displacement curve gives valuable information about the phase transformation, cracking and delamination of the films, in addition to hardness and the elastic modulus of the material.

Parameters	Formula
Elastic Modulus	Reduced elastic modulus (E*) can be expressed as: $E^* = \frac{1}{2}\frac{\sqrt{\pi}}{\sqrt{Ac}}\frac{dp}{dh}$……………………………………………(1) • A_C is the residual projected area of contact between the indenter and the sample. • dp/dh is the slope of the unloading curve at maximum load.
Hardness	the hardness (H) can be expressed as: $H = \frac{P_{max}}{Ac}$……………………………………………(2) • P_{max} is the maximum applied load • For an ideal Berkovich indenter, $A_C = 24.5h_c^2$ $h_c = h_{max} - \omega\frac{P_{max}}{S}$……………………………………………(3) • h_{max} is the displacement at maximum load • ω is a constant and its value for the Berkovich indenter is 0.75.
Plastic Resistance parameter	H/E……………………………………………………(4) • H/E varies in the range of 0.0 and 0.1
Elastic recovery (ER)	$\% ER = \frac{h_{max}-h_{res}}{h_{max}} \times 100$……………………………(5) • h_{max} is the displacement at maximum load • h_{res} is the residual displacement after removing the loads
Plastic deformation energy (U_r)	$U_r = \left[\frac{1}{3}\sqrt{\frac{1}{\omega_o \tan^2\Psi}}\right]\frac{1}{\sqrt{H}}P^{3/2}$………………………(6) • w_o is the geometry constant and attained the value of 1.3 for the Berkovich indenter, • P is the load • ϕ is the half angle of the Berkovich indenter that has the value of 65.3°.

Table S1. Formulas extracted from load displacement curve by using Olive Pharr model.

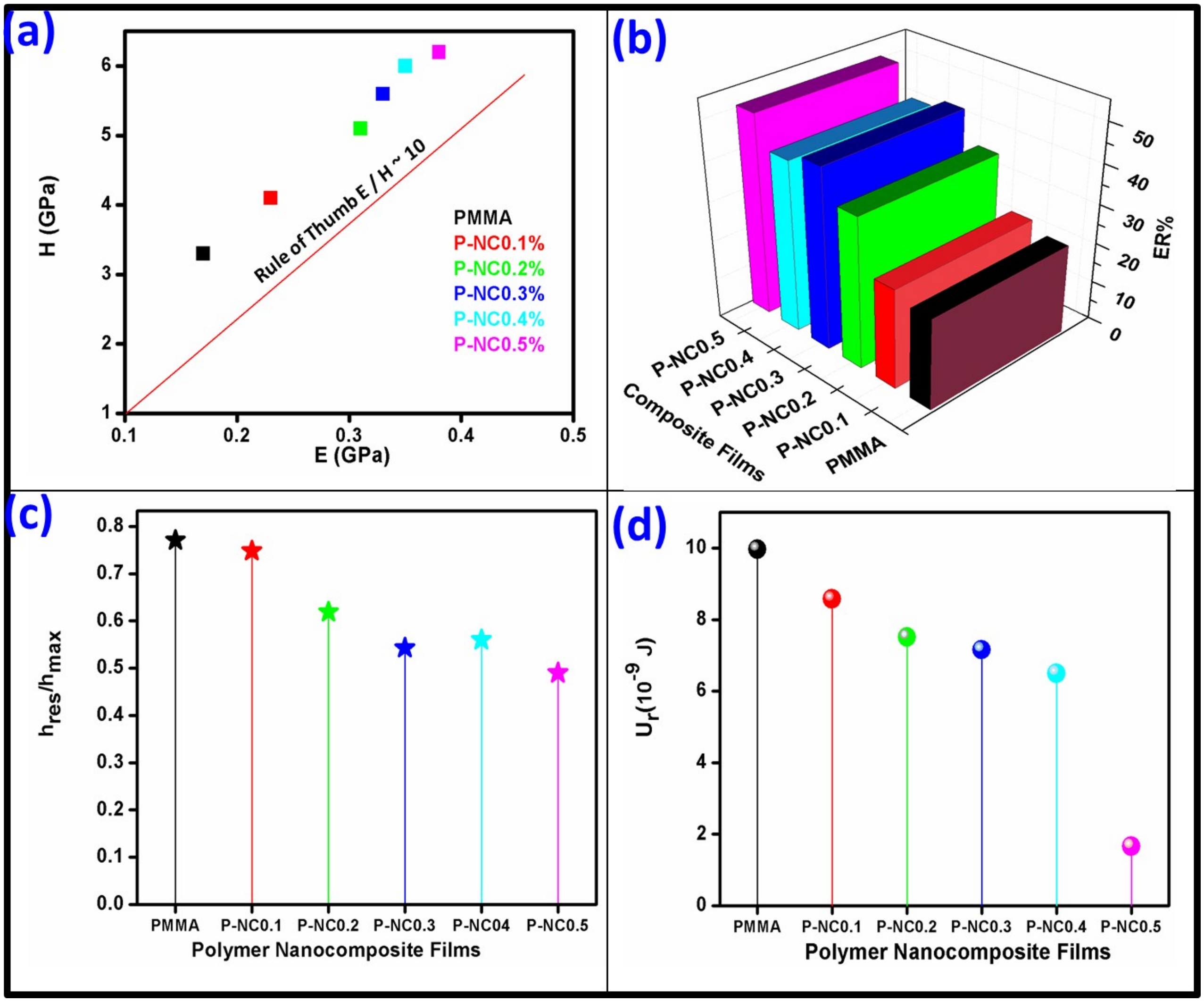

Figure. S8 (a) Plot of H versus E curve for P-NCs. **(b)** Variation of % elastic recovery (ER) for P-NCs with different NGP loadings. **(c)** h_{res}/h_{max} of P- NCs at 1 mN indentation load. **(d)** Variation of plastic deformation energy (U_r) for P-NCs with different NGP loadings.

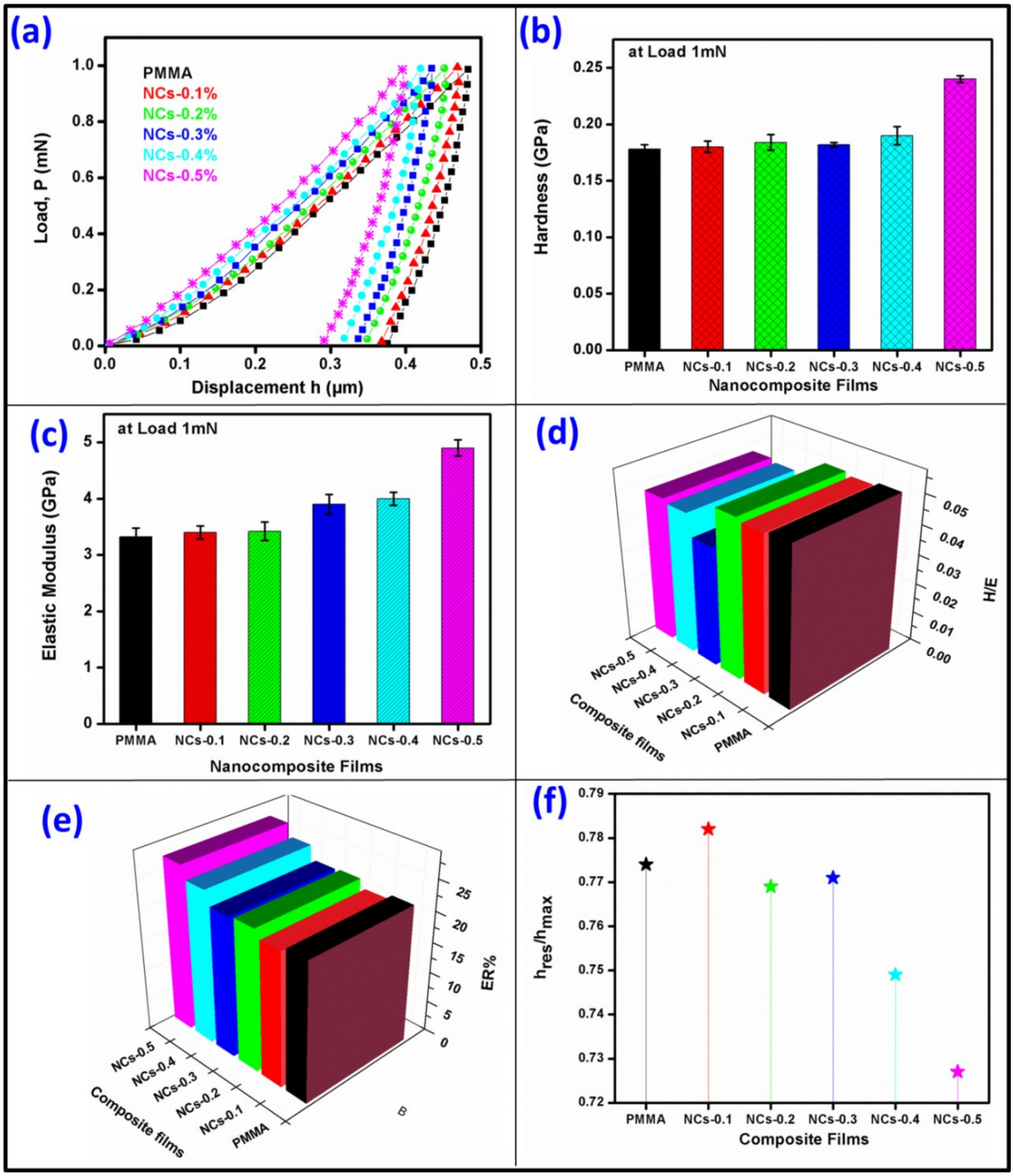

Figure S9. (a) Load versus displacement curves of pure PMMA and NCs prepared by the physical mixing of PMMA with different NGP wt% (NCs-0.1, NCs-0.2, NCs-0.3, NCs-0.4 and NCs-0.5) at 1mN load. (b) Measurement of hardness as a function of NGP loading in wt %. (c) Variation of elastic modulus with NGPs loading. (d) Plastic resistance parameter (H/E) at 1 mN Load. (e) Variation of % elastic recovery (ER) for NCs with different NGP loadings. (f) h_{res}/h_{max} of NCs at 1 mN indentation load.

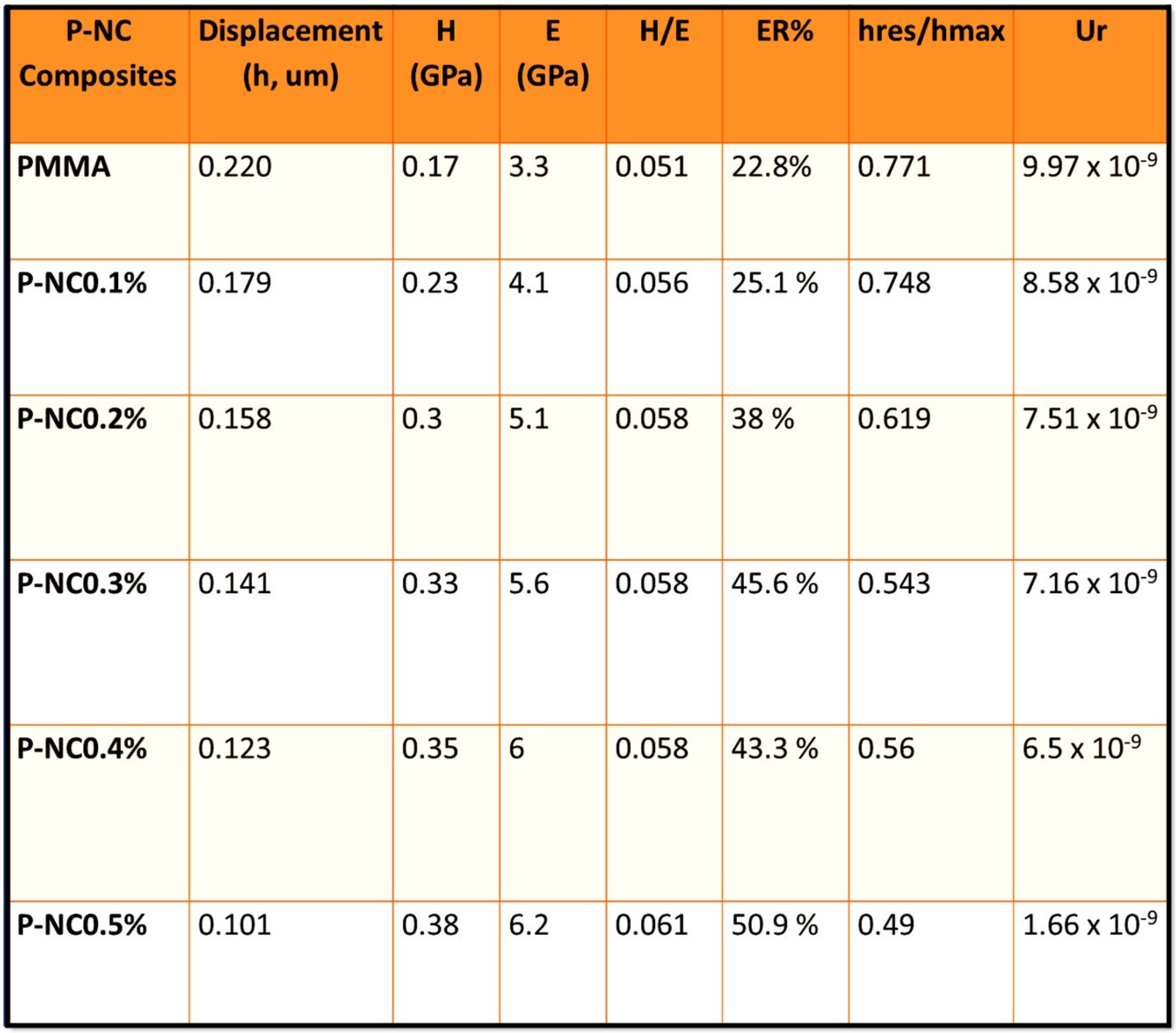

P-NC Composites	Displacement (h, um)	H (GPa)	E (GPa)	H/E	ER%	hres/hmax	Ur
PMMA	0.220	0.17	3.3	0.051	22.8%	0.771	9.97 x 10^{-9}
P-NC0.1%	0.179	0.23	4.1	0.056	25.1 %	0.748	8.58 x 10^{-9}
P-NC0.2%	0.158	0.3	5.1	0.058	38 %	0.619	7.51 x 10^{-9}
P-NC0.3%	0.141	0.33	5.6	0.058	45.6 %	0.543	7.16 x 10^{-9}
P-NC0.4%	0.123	0.35	6	0.058	43.3 %	0.56	6.5 x 10^{-9}
P-NC0.5%	0.101	0.38	6.2	0.061	50.9 %	0.49	1.66 x 10^{-9}

Table S2. Nanomechanical properties of the P-NC films with different NGP (wt%) loadings.

Matrix	Nanofiller type	Processing method	Nanofiller content %	Elastic Modulus (GPa)	Hardness (GPa)	Reference (Year)
PMMA	Amide-f-FG	Ultrasonication	0.2% 0.4% 0.6%	3.36 3.61 3.65	0.144 0.145 0.153	B. Das et. al.[1] (2009)
PMMA	Nanosilica 3nm	Silanization of SiO2 sonication In-situ polymerization Thermal curing	3 3(SC gel) 3(SC gel)	3.88 3.88 4.56	0.258 0.276 0.326	D. Stojanovic et. al. [2] (2009)
PMMA	Graphene-like boron nitride	Sonicated in Chloroform solvent Sonicated in DMF solvent	3% 3%	4.41 3.42	0.250 0.195	M. S. R. N. Kiran et al.[3] (2010)
PMMA	Expanded Graphene (EG)	Melt-blending	0.25% 0.5% 1.0%	4.5 4.7 4.7	0.45 0.51 0.49	H. Chakraborty et. al.[4] (2012)
PMMA	ZnO	In-situ spin coating	0.25% 0.5% 1%	4.3 5 4.2	0.38 0.4 0.37	H. Chakraborty et. al.[5] (2013)
PMMA	Covalently-functionalised graphene (FG)	In-situ copolymerisation	0.2% 0.4% 0.6% 1%	3.7 4.7 5.4 5.5	0.17 0.19 0.23 0.25	Yingkui Yang et al.[6] (2014)
PMMA	Nanographite Platlets (NGPs)	Click Chemistry	0.1% 0.2% 0.3% 0.4% 0.5%	4.1 5.1 5.6 6.0 6.2	0.23 0.3 0.33 0.35 0.38	This work

Table S3. A comparison of the nanomechanical properties of PMMA nanocomposites reported in literature through nanoindentation technique.

2. Preparation of Sensor Device and Sampling System

The conductivity of the films with different NGP wt% was measured by two point probe Keitley 6517 B electrometer within the potential window of -10V to 10V. The principle of the operation of the chemiresistive sensor is mainly based on the resistance change with the adsorption of the target gas by the P-NCs materials. The sensing measurement were conducted at room temperature in a sealed chamber with total volume of 5 L. The temperature was monitored by a mercury thermometer. Two ohmic contacts were made on each of the film using silver paste with 0.1mm spacing between the contacts. The resistance of the sensor was recorded continuously which was interfaced to the computer. When the electrical resistance of the P-NC approached its equilibrium value, the vapor of ammonia was removed from the closed vessel with the flow of air in order to clean the sensor environment. The measured data were analysed and plotted in the form of response curves.

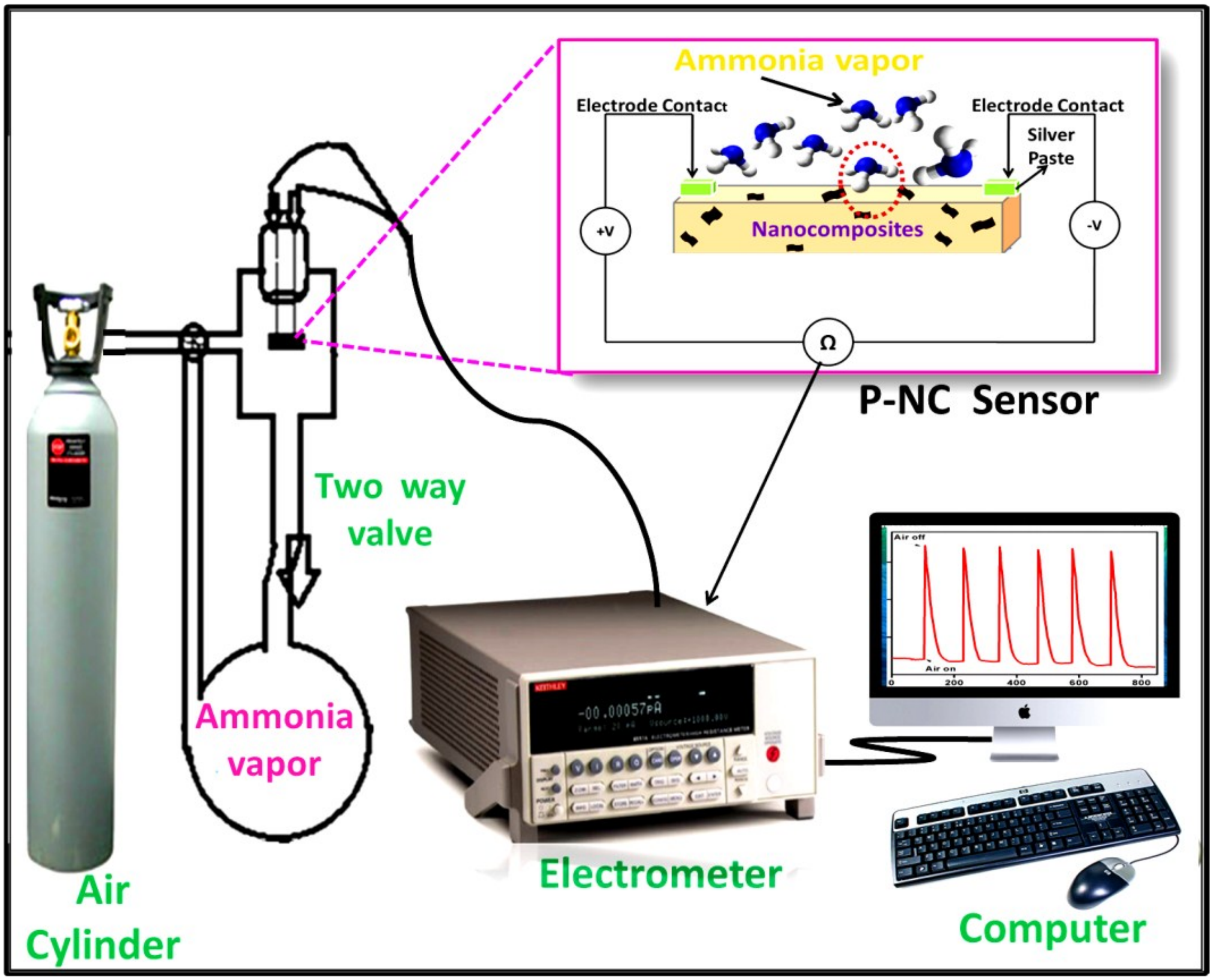

Figure. S10 Experimental set-up for ammonia vapor sensing using flexible P-NC sensor.

Figure. S11 Comparative test to check the specificity of ammonia vapor to P-NCs.

REFERENCES

[1] B. Das, K. E. Prasad, U. Ramamurty and C.N.R. Rao, *Nanotechnol.*, 2009**, 20**, 125705-125710.

[2] D. Stojanovic, A. Orlovic, S. Markovic, V. Radmilovic, P. S. Uskokovic and R. Aleksic, *J. Mater. Sci.,* 2009**, 44**, 6223-6232.

[3] M.S.R.N. Kiran, Kalyan Raidongia, U. Ramamurty and C.N.R. Rao, Scripta Mater., 2011, **64**, 592-595.

[4] H. Chakraborty, Arijit Sinha, Nillohit Mukherjee and Partha Protim Chattopadhyay, *J. Nanotechnol*., 2012, doi:10.1155/2012/940516.

[5] H. Chakraborty, Arijit Sinha, Nillohit Mukherjee, Dipa Ray and Partha Protim Chattopadhyay, *Materials Letters*, 2013, 93, 137-140.

[6] Y. Yang, C. He, Wei Tang, C. P. Tsui, D. Shi, Z. Sun, T. Jianga and X. Xiec, *J. Mater.Chem.*, 2014, **2**, 20038-20047.